ATLAS Internal Note
MUON-NO-xxx

29 October 1997

Influence of aqueous vapour on the drift properties of MDT gases

S. Kircher, V. Paschhoff, G. Scherberger, G. Herten, U. Landgraf, W. Mohr
University of Freiburg*

N. P. Hessey, M. Deile.
University of Munich†

June 97

ABSTRACT

We present a systematic investigation of the influence of aqueous vapour on the electron drift properties of MDT gases. Measurements on the drift gases Ar, CH_4, N_2 $(91, 5, 4)$, called the DATCHA gas, and Ar, CH_4, N_2, CO_2 $(94, 3, 2, 1)$ were performed at the ATLAS testbeam in H8. A silicon telescope was used as an external reference system for the MPI 4x4 drift chamber, which was put into a 1 Tesla magnet.
For each gas we give the maximum drift time, the magnetic field dependence and the resolution drop due to water content instabilities as a function of the water content.
We conclude that the drift properties of the DATCHA gas, concerning the water content, have an optimum at about 1900 ppm, while for the the second gas a region between 700 and 1800 ppm seems favourable.

*Address: Fakultät für Physik, Hermann-Herder-Str. 3, 79104 Freiburg i. Br., Germany
e-mail: kircher@physik.uni-freiburg.de
†Address: Sektion Physik, Schellingstr. 4, 80799 München, Germany

1 Introduction

Previous experiments with MDT's showed inconsistencies or a lack of reproducibility concerning the electron drift properties, if Rilsan hoses were used as gas connections. Since Rilsan is known to outgas H_2O [KOLL96] the uncontrolled water content was assumed to be the reason for it. Furthermore the MAGBOLTZ prediction of the drift properties for gases with a small water content was known to be poor [HILD95]. Both, the experiment and the simulation, led to the following assumptions

- the electron drift properties of MDT gases strongly depend on the water content
- the maximum drift time as a function of the water content has a minimum at a certain amount of H_2O vapour in the gas.
- water reduces the Lorentz angle

The question arose whether the dependence of the drift properties on the water content and hence the contribution to the resolution drop is minimal at a certain water content. Furthermore it seemed interesting to study if adding aqueous vapour to the MDT gas could optimise the linearity of the space to drift time relationship and to what extent the Lorentz angle could be reduced. Apart from a possible improvement of the drift properties the water content is believed to be helpful against wire chamber ageing [KADY90] and known to preserve the mechanical and electrical isolating properties of plastic parts [KEME95].
We concluded that a systematic investigation where all parameters but the water content and the magnetic field are fixed became necessary.
In this note we describe the experimental setup in H8 and the method of analysis. We then present the results and discuss their implications for ATLAS.

2 Experimental Setup

The measurements of the drift properties were performed at the ATLAS test beam area H8 in spring 1997. We investigated the gases Ar, CH_4, N_2 $(91, 5, 4)$, which is known as the DATCHA gas and Ar, CH_4, N_2, CO_2 $(94, 3, 2, 1)$, which will be referred to as the four component gas in the following.
Aqueous vapour has been mixed to the drift gas by splitting the gas flow from the supply into a fraction that remained unchanged and second one that was mixed with water vapour in a bubbler (figure 1). A temperature conditioner was used to keep the bubbler at a temperature of $14\,^oC$, which at 3 bar corresponds to a water content of ≈ 5300 ppm (assuming 100 % saturation). Since the saturation in the bubbler was about 80 % efficient (figure 6), any water content between 0 and 4500 ppm could be maintained in the drift chamber, by changing the ratio of the gas flows. The water temperature was permanently measured with a pt100 thermo coupler at the bubbler, while the water content was monitored just before the chamber with

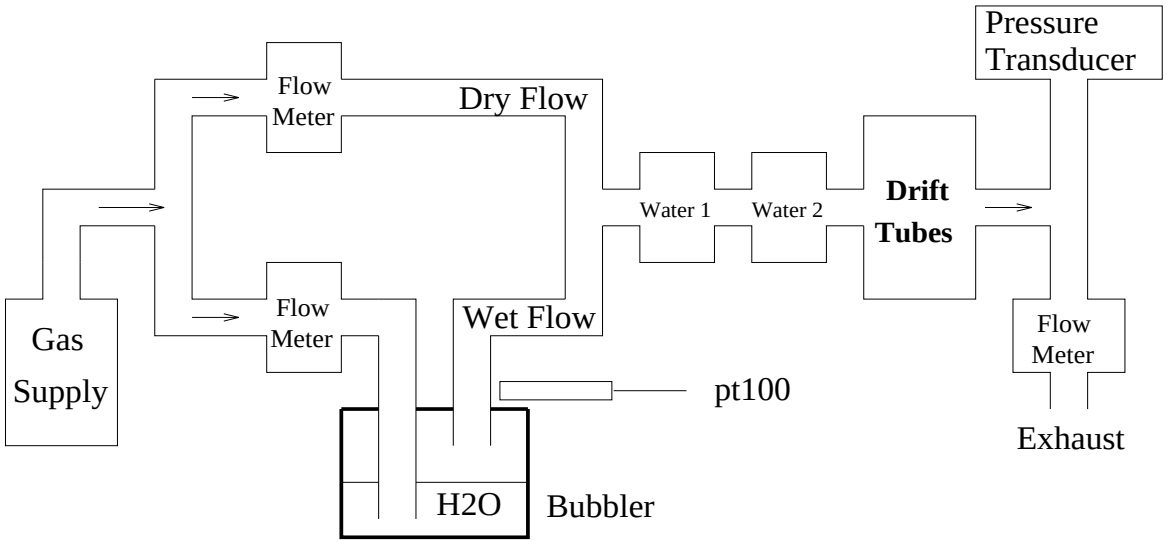

Figure 1: Schematic view of the gas system. A fraction of the gas is moistened in a bubbler to have a variable water content in the drift chamber. It is monitored with two Endress & Hauser Alphasensors.

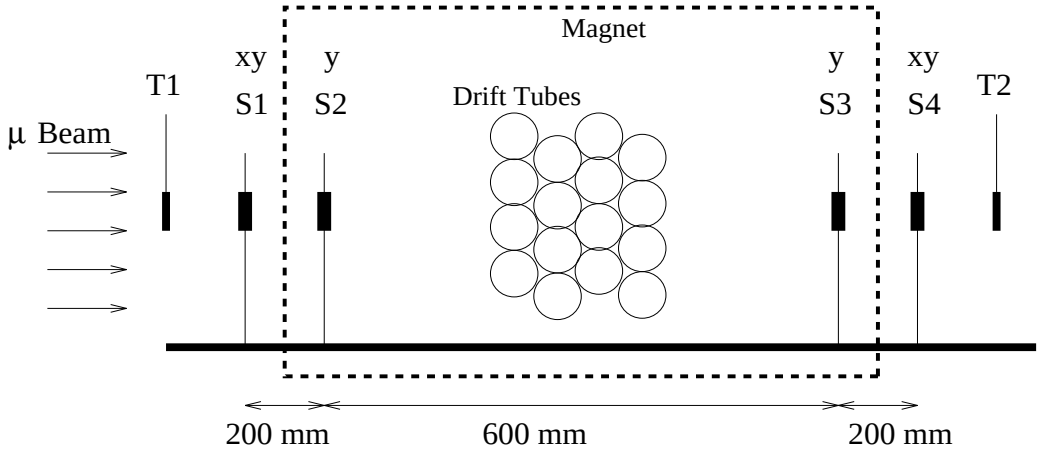

Figure 2: Setup of the detectors. T_1 and T_2 are two scintillators in coincidence. S_1 to S_4 are the four planes of the silicon telescope. The two inner planes measure in y-direction while the outer ones measure in x and y direction. The drift tubes are in a 1 Tesla magnet.

two Endress & Hauser DY 73 Alphasensors. They are designed to measure the dewpoint with an accuracy of $\pm 1\,^{o}$C.
The setup of the detectors consists of four major parts:

- a drift chamber with 16 tubes
- a silicon microstrip detector with six planes as an external reference system
- two scintillators in coincidence as a trigger

detector	parameter	value
silicon telescope	sensitive area	$51 \times 51\,\mathrm{mm}^2$
	planes in x / y	2 / 4
	resolution	$< 10\,\mu\mathrm{m}$
drift tubes	wire length / diameter	98 mm / $50\,\mu\mathrm{m}$
	wire material	W Re
	inner radius	14.75 mm
	wall thickness	0.250 mm
	pressure	3 bar
trigger	sensitive area	$52 \times 52\,\mathrm{mm}^2$
magnet	maximum field	1 Tesla
DATCHA gas	Ar, CH_4, N_2	91 % 5 % 4 %
	HV / gas gain	3270 Volt / $2 \cdot 10^4$
4 component gas	Ar, CH_4, N_2, CO_2	94 % 3 % 2 % 1 %
	HV / gas gain	3130 Volt / $2 \cdot 10^4$

Table 1: Summary of important detector and gas parameters

- a magnet with a field of up to 1 Tesla

Four of the six planes of the silicon telescope measure the y-coordinate, which was the precision coordinate, with a resolution of $< 10\,\mu$m. The other two planes measure the x-coordinate, which is the direction along the wire. For details about the setup please refer to figures 1 and 2 as well as table 1 while a detailed description about the silicon telescope can be found in [DUBB96]. The gas gain for both gases was chosen according to the ATLAS baseline of $2 \cdot 10^4$. This corresponds to a high voltage of 3270 Volt for the DATCHA gas [MN122] and 3130 Volt for the four component gas. The latter was obtained by comparing the ADC-spectra of both gases in the Freiburg ageing setup.

3 Method of Analysis

3.1 Determination of the rt-Relation

Determination from the measurement :

We determine the space to drift time relationship (rt-relation) with an iterative method by computing the residuum Δt in a space region (figure 3). The residuum Δt is defined as the difference between the drift time t_{tdc} and the silicon telescope time t_{stel}

$$\Delta t \quad = \quad t_{tdc} - t_{stel} \quad = \quad t_{tdc} - t(r_{stel})$$

t_{stel} is obtained from the silicon telescope track r_{stel} using the rt-relation. The new rt-relation is calculated by using the mean of the residuum in a bin as the correction to the old rt-relation

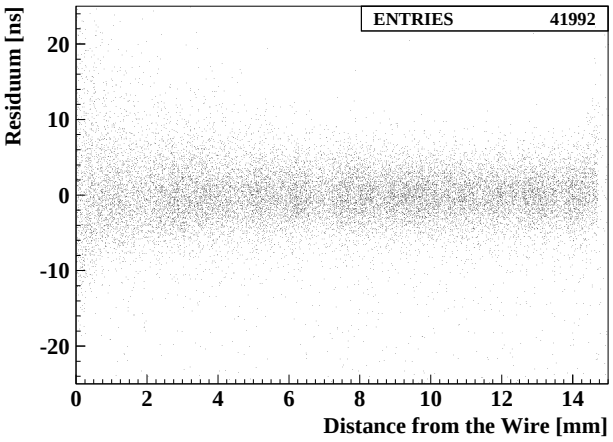

Figure 3: The residuum Δt plotted against the radius obtained from the silicon telescope r_{stel}.

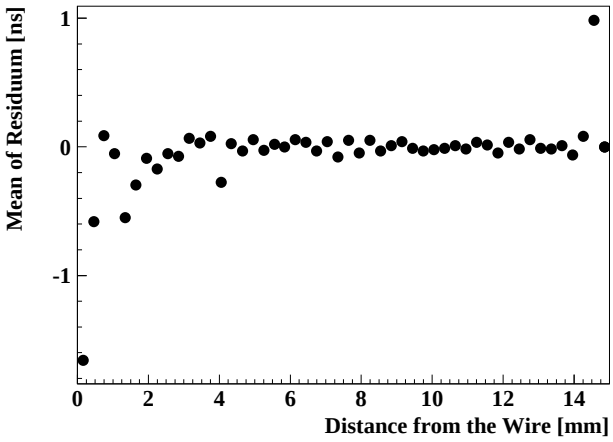

Figure 4: The mean of the residuum distribution is calculated in bins along the radius and used as a correction for the rt-relation.

(figure 4). We use a polygon to parameterise the rt-relation.
Since the residuum distribution has approximately a Gaussian shape for $r > 2\,\text{mm}$ the mean value in a bin is calculated with a Gauss Fit. The RMS of the mean values in bins with $2\,\text{mm} < r < 14\,\text{mm}$ is after about eight iterations given by RMS $= \frac{\sigma}{\sqrt{N}}$, if N is the average number of entries in a bin and σ the average width of the Gauss-fit. For a more detailed description see [SAMM97].

Determination with a simulation :

In addition to the measurements, GARFIELD/MAGBOLTZ simulations [VEEN97a] of rt-relations were performed for both gases. A temperature of $20\,^{o}\text{C}$ was assumed. All other input parameters were chosen according to table 1.
For simplicity the simulation was done without taking effects like diffusion and clustering into account. The resulting difference between this simulation and the one that takes the above effects into account can be up to 20 ns [VEEN97b].

3.2 Determination of the Maximum Drift Time

There are many ways to define the maximum drift time. E.g. the time between the passage of a muon at the outer edge of the tube and the arrival of the first electron at the wire. This definition is for the following reasons not very practical

1. the time of the muon passing is not known
2. at the outer edge of the tube the efficiency is zero [MN137]

A more practical way is to measure the width of the drift time distribution. But we

1. do not know which points of the spectrum to call start and end.

2. need to allow for a correction of the inefficiency at the wall.

We determine the maximum drift time by two methods: a fit to the whole drift time distribution using Fermi functions and secondly measuring the rt-relation and extrapolating it to the outer edge of the tube. A comparison of both methods is presented in section 4.1.
In order to have a common systematic error for simulation and measurement, the maximum drift time was calculated in both cases with the extrapolation method.

3.2.1 Fermi Method

To measure the width of the drift time distribution we fit slightly modified Fermi functions, $N_r(t)$ and $N_f(t)$, to the rising edge and the falling edge of the spectrum* (See figure 5):

$$N_r(t) = \frac{R_3 + R_4 \cdot e^{\frac{-t}{R_5}}}{\left(1 + e^{\frac{R_1 - t}{R_2}}\right)}, \qquad N_f(t) = \frac{F_3}{\left(1 + e^{\frac{F_1 - t}{F_2}}\right)} \tag{1}$$

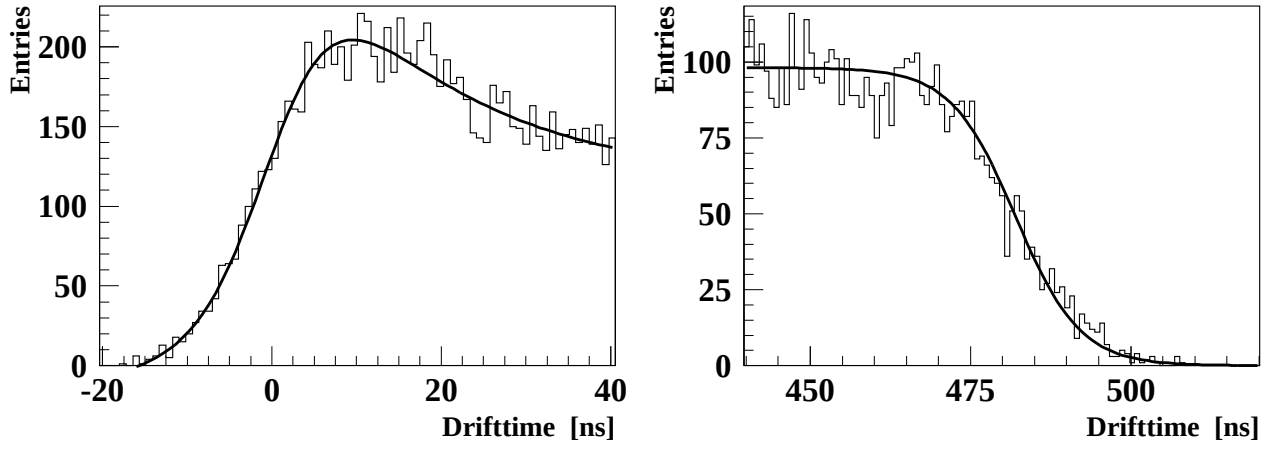

Figure 5: Fit to the drift time distribution using Fermi functions. $N_r(t)$ is fitted to the rising edge and $N_f(t)$ to the falling edge of the spectrum.

where F_1 is the time that corresponds to the half height of the falling edge, while R_1 is approximately the time of half height of the rising edge (modified by $R_4 \cdot e^{\frac{-t}{R_5}}$). F_2 and R_2 describe the slope of the edges. Without the exponential component in $N_r(t)$, the fit often fails, and the

*If the drift time distribution is flat both fits can be made simultaneously [MN158].

R_1 parameter becomes very dependent on the range of the fit.
The maximum drift time in the Fermi method is then defined as

$$t_{max} \quad := \quad (F_1 + \alpha F_2) - (R_1 + \beta R_2) \tag{2}$$

where α and β account for the fact that the maximum drift time is not equal to the time difference between the half height of the rising and falling edges. Four instead of two parameters were used in the hope that further investigations will show that F_2 and R_2 are gas dependent, while α and β are universal. The value of $\beta R_2 = 1.8\,\text{ns}$ was determined with the silicon telescope. For the analysis α was assumed to be zero. In section 4.1 we will show how a better approximation for α can be obtained.

3.2.2 Extrapolation Method

The rt-relation was measured as described in section 3.1. The maximum drift time t_{max} is obtained by extrapolating it to the outer edge of the tube. The extrapolation becomes necessary because the tube is inefficient near the aluminium wall. We apply a linear fit through the last four points of the rt-relation.

3.3 Determination of the Water Content

The measurement of the water content with the given Endress & Hauser Alphasensors is rather difficult since they are only accurate to $\pm 1\,^o$C dewpoint. To give an example the table below lists the accuracy of the water monitor in different ranges for the given dewpoint accuracy.

dewpoint	water content $w \pm \sigma_{dp}$	relative accuracy
-69 ^{o}C $\pm$ 1 ^{o}C	0.995 ppm $\pm$ 0.147 ppm	14.8 %
3 ^{o}C $\pm$ 1 ^{o}C	2498 ppm $\pm$ 177 ppm	7.1 %
13 ^{o}C $\pm$ 1 ^{o}C	5258 ppm $\pm$ 645 ppm	13.3 %

Because of the difficulties we investigated whether the alphasensors are consistent within the design limits and compared their measurement with the expected water content (figure 6). The latter was calculated from the ratio of both gas flows, the temperature measured at the bubbler and the assumption, that the gas in the bubbler is 100 % saturated. The expected value is therefore an upper limit for the actual water content.
The agreement between the alphasensors was within the design limit except for the range of 0 to 100 ppm. To determine the agreement between expected and measured value we calculated their ratio, which can be regarded as the level of saturation in the bubbler. The fact that the saturation remains at about 80 % is another proof of the reliability of the water measurements.
The water content during one run is calculated by averaging over both alphasensors and all slow control entries during the run. Its error is the quadratic sum

$$\delta w \quad = \sqrt{\quad \sigma^2_{RMS} \quad + \quad \sigma^2_{dp}} \tag{3}$$

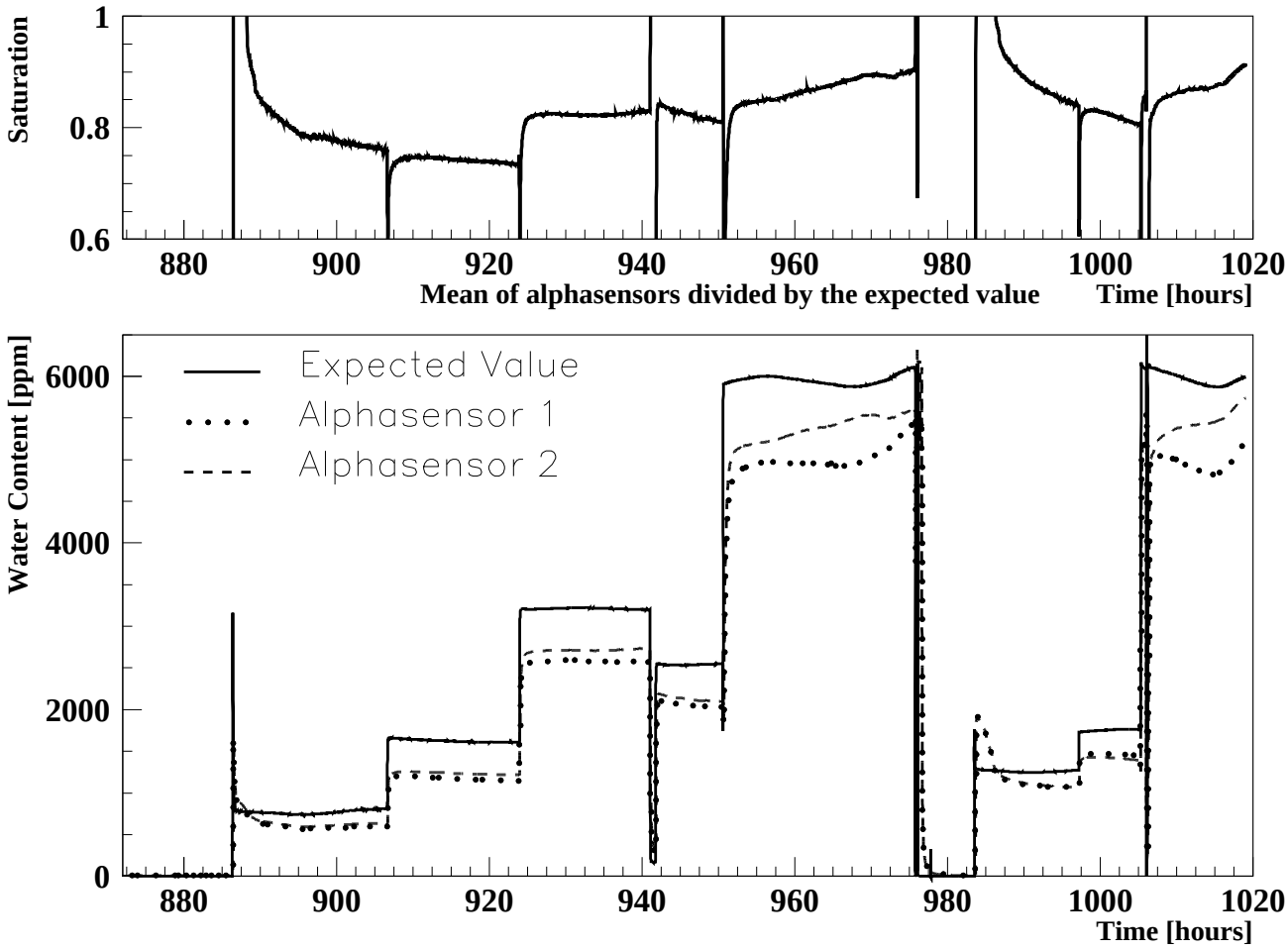

Figure 6: Water Monitor Studies. The upper graph shows the saturation level of the bubbler, the lower one the calculated and measured water content.

where σ_{RMS} is the RMS of the slow control entries and σ_{dp} the contribution from the accuracy of the water monitor. The higher the water content the more important the contribution from σ_{dp} becomes. At 20 ppm σ_{dp} is about twice as big as σ_{RMS} while at 4500 ppm it is about 30 times bigger. δw is the uncertainty of the water content shown in the figures 8 to 13 and 14 to 16.

3.4 Resolution Drop due to Water Content Instabilities

We investigated the contribution to the resolution drop of the drift tube due to water content instabilities Δw. An estimate for this contribution is the RMS difference $D_{\Delta w}(w)$ of an rt-

relation with a water content of w and a second with a water content of $w + \Delta w$

$$D_{\Delta w}(w) \quad = \quad \sqrt{\frac{1}{N}\sum_{i=1}^{N}\Big(r_w(t_i) - r_{(w-\Delta w)}(t_i)\Big)^2} \tag{4}$$

where the sum goes over all polygon points of the rt-relation and $r_w(t_i)$ is the drift distance that correspond to the polygon point i.
For water contents between those at which measurements were made, $r_w(t_i)$ was obtained by interpolation with spline fits.

4 Results

4.1 Comparison of Fermi and Extrapolation Method for the Maximum Drift Time

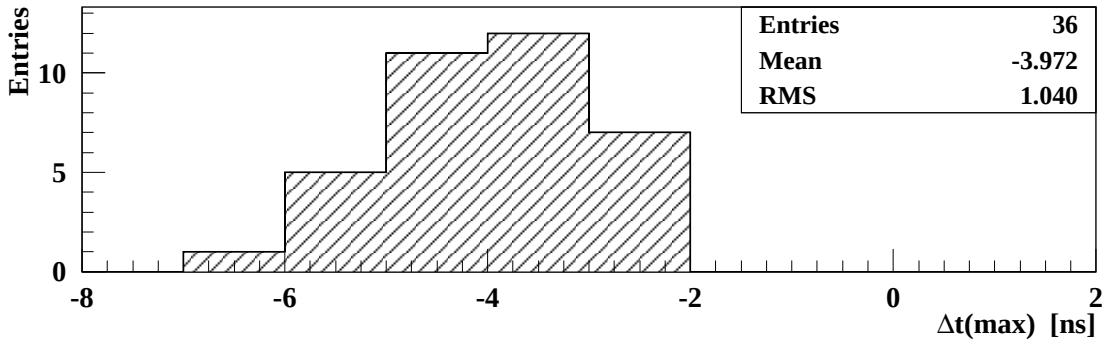

Figure 7: Comparison of Fermi and Extrapolation Method. The graph shows the distribution of the difference of the maximum drift time Δt_{max} obtained with the Fermi- and the Extrapolation method. The entries are taken from the DATCHA gas at 0.0 and 0.6 Tesla.

We calculated the maximum drift time with the Fermi and Extrapolation method. The difference $\Delta t_{max} = t_{max_{fermi}} - t_{max_{extrap}}$ was histogrammed in figure 7 for all fully illuminated tubes of the DATCHA-gas at 0.6 and 0.8 Tesla. This difference has a slight dependence on drift gas, B-field and water content, and the spread is partly due to these systematics. The choice of this data sample in figure 7 is a compromise between high statistics and a data sample without systematics.
The RMS of 1.0 ns is therefore the combined error of both methods and an upper limit for the error of each method. It accounts for the random error as well as the systematic error. The random errors of each method sum up to ≈ 0.3 ns, which is more than a factor of three smaller than the RMS.
This discrepancy is not fully understood. It is partly explained by the following

- we extrapolate into the blind area of the tube, where we have no information how the rt-relation behaves. The systematic error of doing so might depend on the water content and therefore appears as a random error in the Δt_{max} distribution.
- The parameter βS_2 could be water content dependent, which could result in a broadening of the distribution 7
- even though a clear trend is not seen, there is enough evidence that different tubes at the same run do not have identical rt-relations (change of drift gas composition through leaks, misalignment of the wire with respect to the wall).

As long as we do not fully understand the above we consider the error of the maximum drift time to be 1.0 ns in the following.
To have a better approximation of the parameter α (equation 2) it can be chosen such that the mean difference of the Fermi and Extrapolation method is zero. That would give a value of $\alpha F_2 = 4.0\,\text{ns}$.

4.2 Water Content Dependence of the rt-relation

The Extrapolation method was used to calculate the simulated and measured time to drift a distance of 5, 10 and 14.75 mm. The results as a function of the water content are shown separately for each gas and magnetic field in figures 8 to 10 (DATCHA gas) and 11 to 13 (four component gas). The error of the drift time comes from the comparison of both methods to determine the maximum drift time; while the inaccuracy of the water content δw was calculated using equation 3. Selected rt-relations were included into the figures to show that the linearity of the rt-relation can indeed be improved through water.
The maximum drift time as a function of the water content has a minimum for each gas and magnetic field. This behaviour disappears for shorter drift distances. The approximate position of the minimum is summarised in table 2. Please note that the agreement between simulation and measurement is poor in some cases, even when the simulated curve is corrected (section 3.1).

B-field	DATCHA Gas	four component gas
0.0 Tesla	≈ 2000 ppm	≈ 500 ppm
0.6 Tesla	≈ 1900 ppm	≈ 700 ppm
0.8 Tesla	≈ 2000 ppm	≈ 1100 ppm

Table 2: Water content giving the shortest maximum-drift-time (measurement).

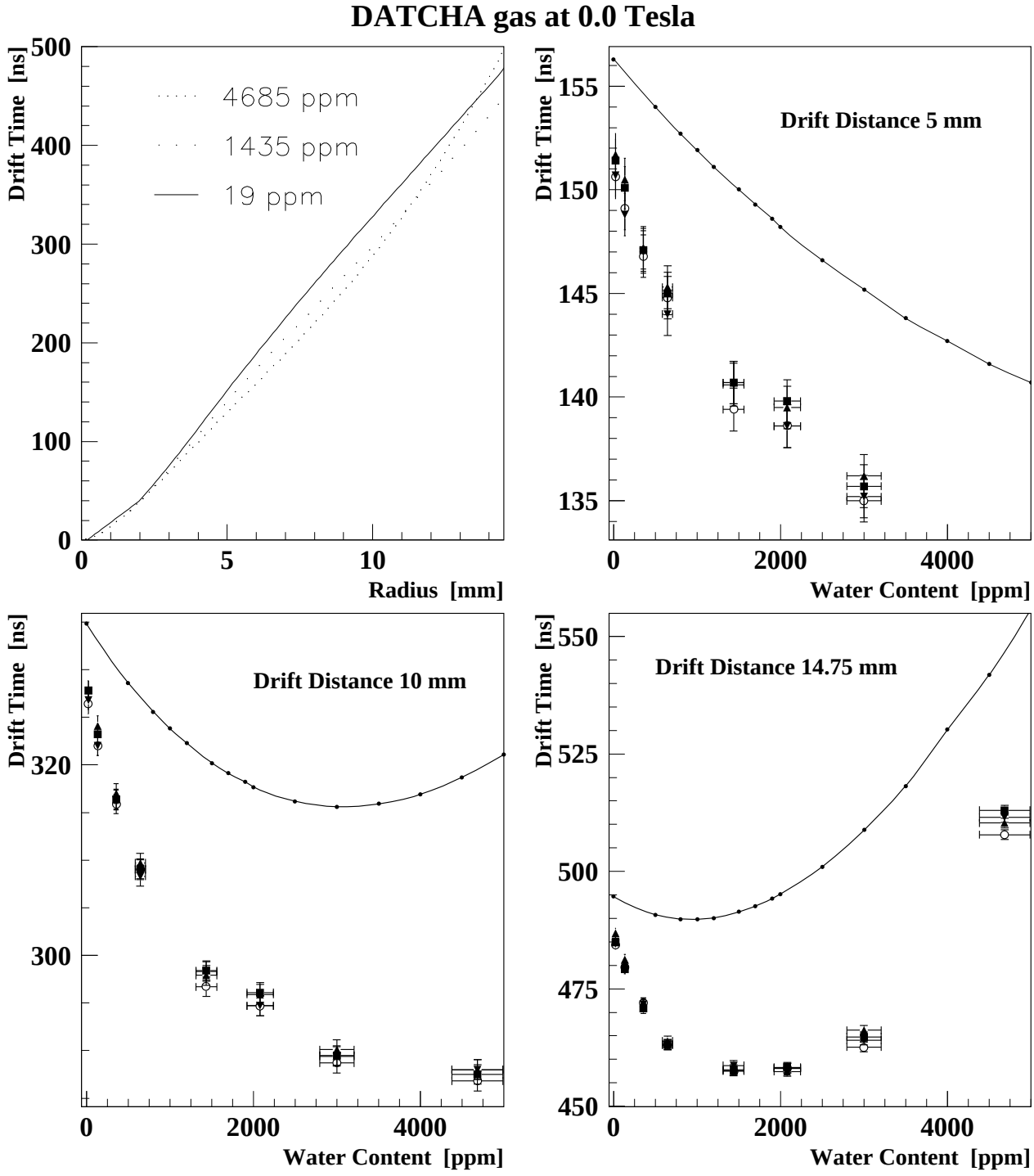

Figure 8: Water dependence of the DATCHA gas at 0.0 Tesla. The upper left plot shows measured rt-relations. The remaining three plots show a comparison between GARFIELD simulation (solid line) and measurement. The various symbols represent different tubes.

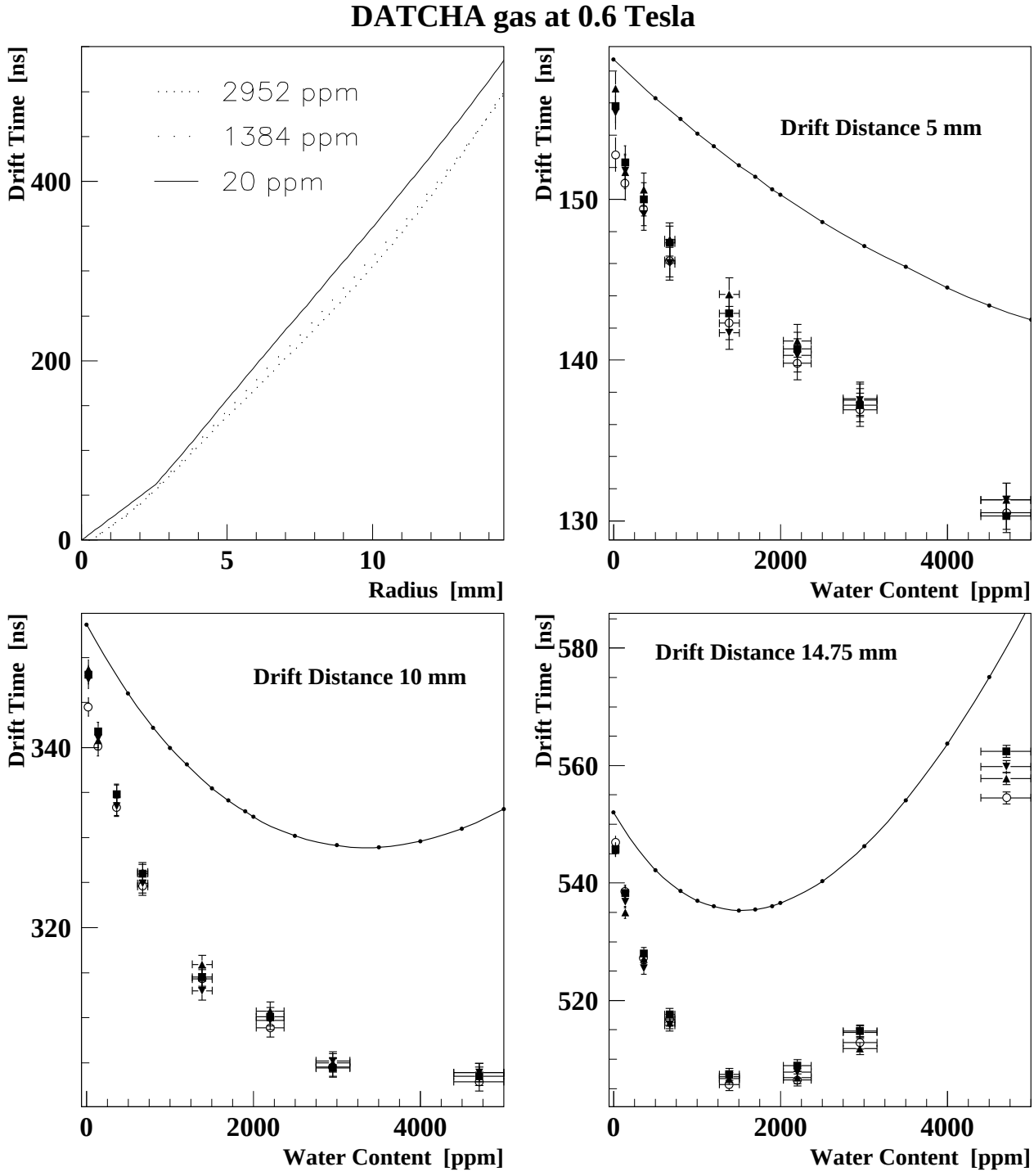

Figure 9: Water dependence of the DATCHA gas at 0.6 Tesla. The upper left plot shows measured rt-relations. The remaining three plots show a comparison between GARFIELD simulation (solid line) and measurement. The various symbols represent different tubes.

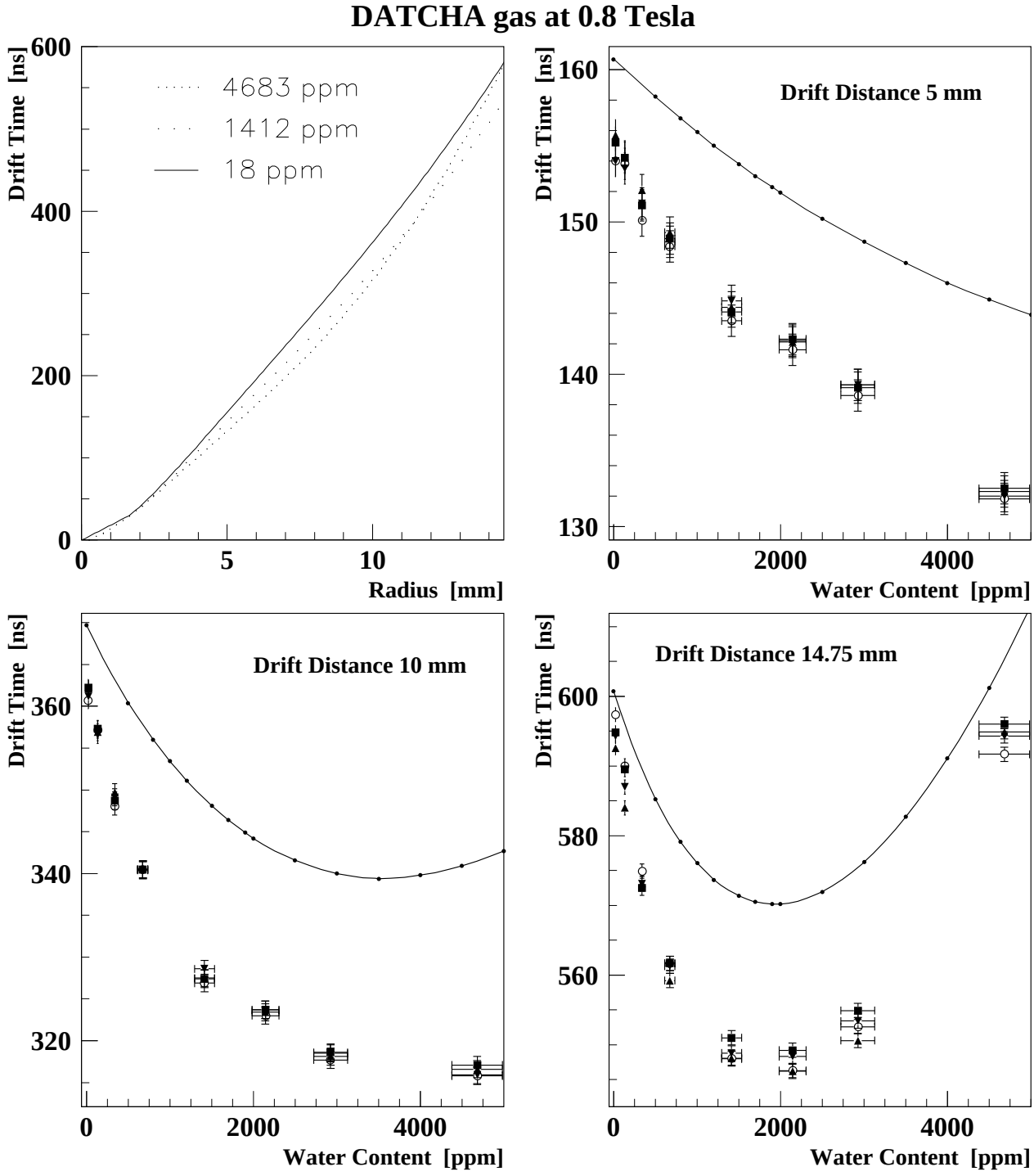

Figure 10: Water dependence of the DATCHA gas at 0.8 Tesla. The upper left plot shows measured rt-relations. The remaining three plots show a comparison between GARFIELD simulation (solid line) and measurement. The various symbols represent different tubes.

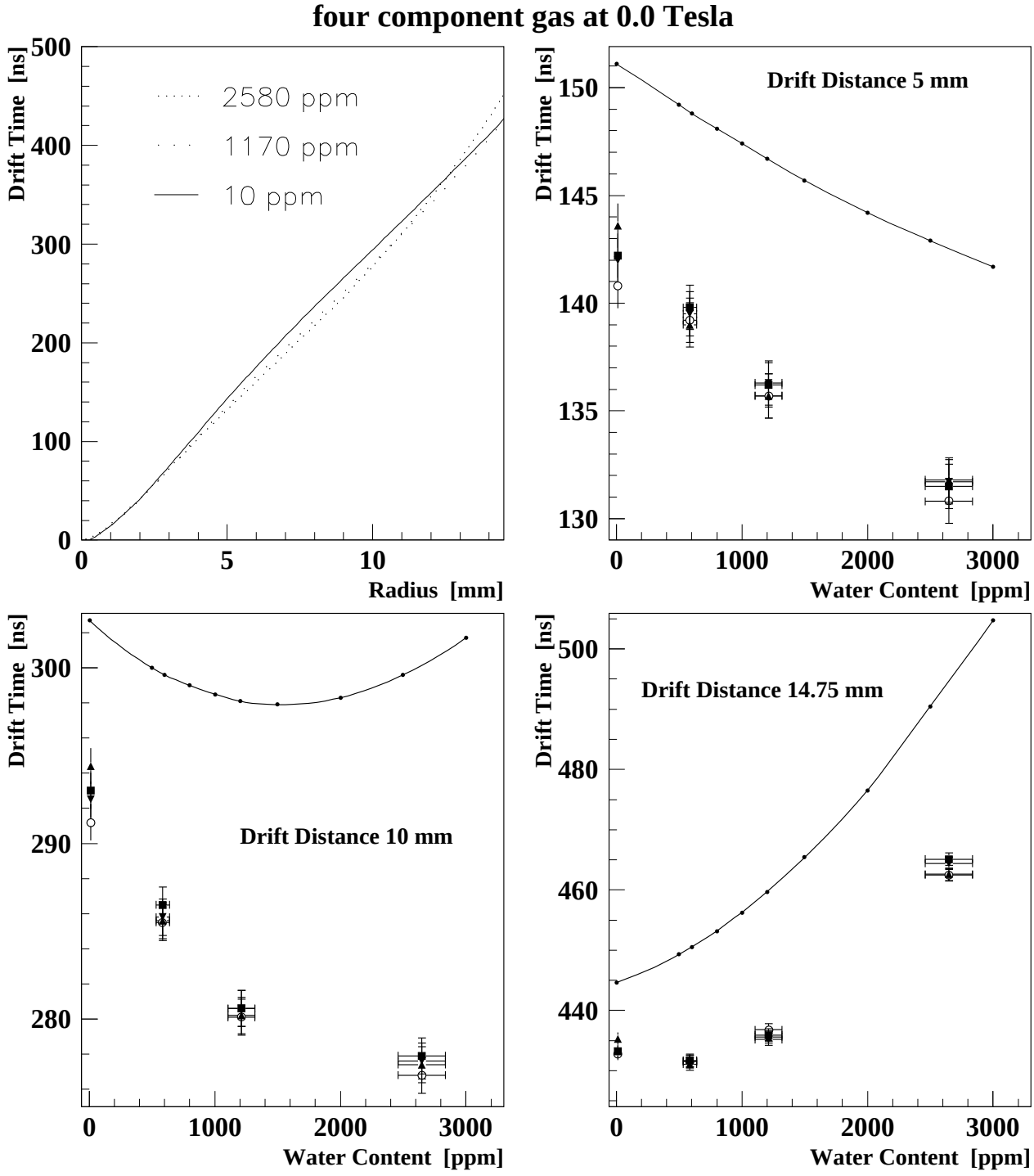

Figure 11: Water dependence of the four component gas at 0.0 Tesla. The upper left plot shows measured rt-relations. The remaining three plots show a comparison between GARFIELD simulation (solid line) and measurement. The various symbols represent different tubes.

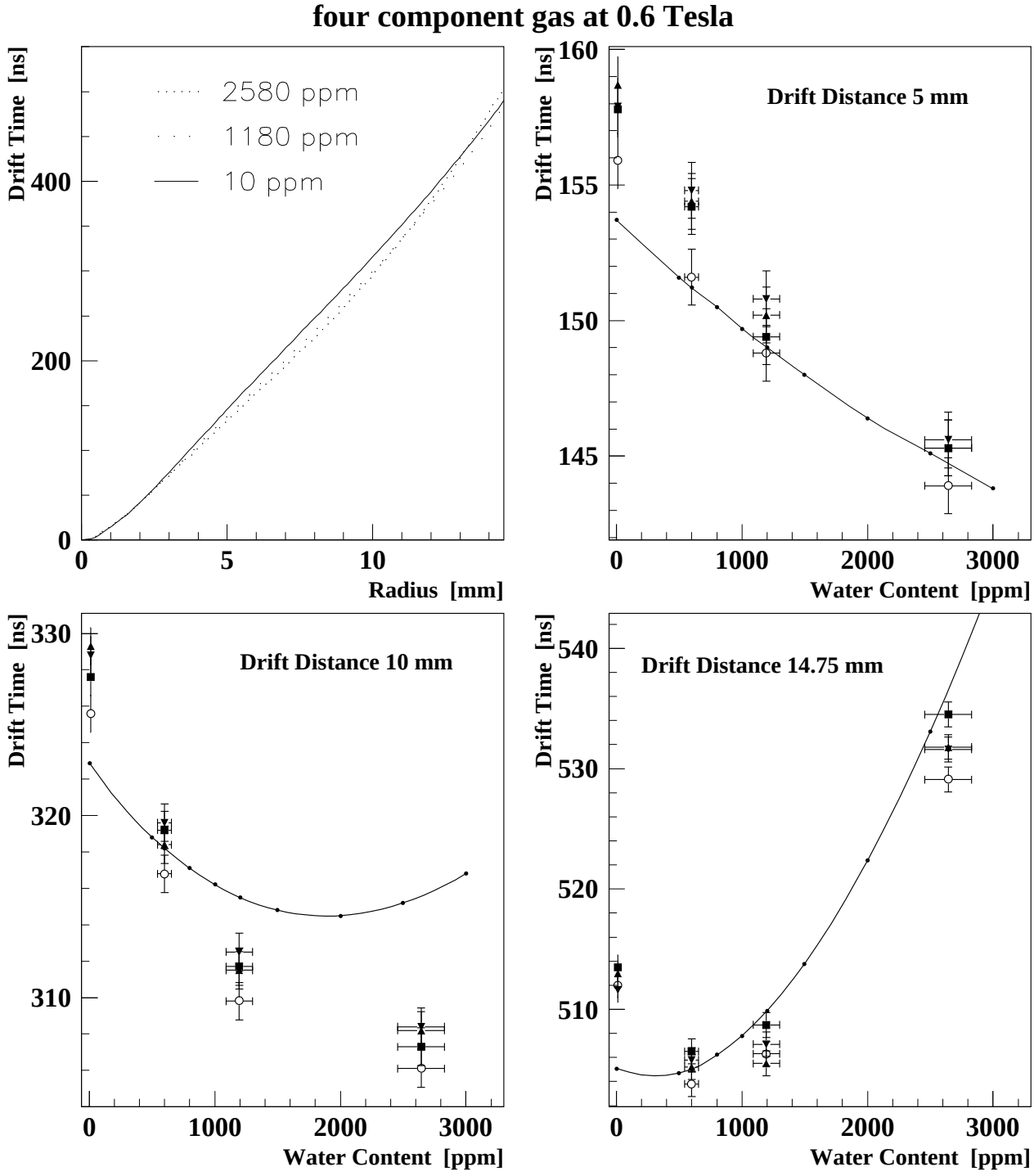

Figure 12: Water dependence of the four component gas at 0.6 Tesla. The upper left plot shows measured rt-relations. The remaining three plots show a comparison between GARFIELD simulation (solid line) and measurement. The various symbols represent different tubes.

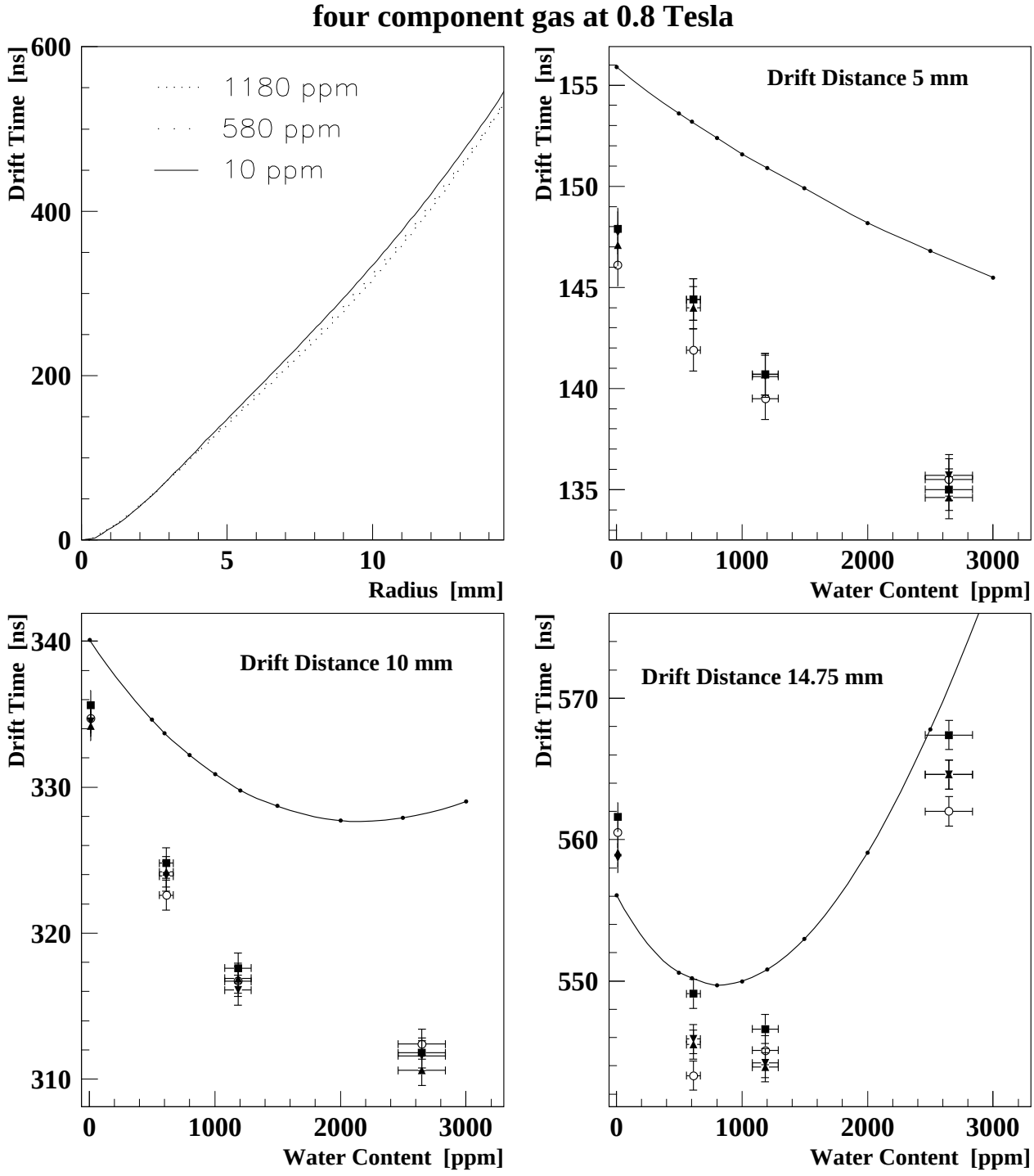

Figure 13: Water dependence of the four component gas at 0.8 Tesla. The upper left plot shows measured rt-relations. The remaining three plots show a comparison between GARFIELD simulation (solid line) and measurement. The various symbols represent different tubes.

4.3 Reduction of magnetic field dependence through water

We calculated the difference of the maximum drift time of two runs with a different magnetic field but the same water content:

$$\Delta t_{max}(w) \quad := \quad t_{max,0.6T}(w) \quad - \quad t_{max,0.0T}(w)$$

where w is the water content. The same calculation was done for 0.8 Tesla as well. The results are shown in figure 14 and 15 for the DATCHA gas and figure 16 and 17 for the four component gas. With increasing water content w, $\Delta t_{max}(w)$ decreases for both gases and both magnetic fields. The relative drop of the B-field dependence for some interesting ranges is listed in table 3.
The drift velocity v_{drift} and therefore Δt_{max} weakly depend on the magnetic field. The main contribution to Δt_{max} is due to the Lorentz angle, which implies that small concentrations of aqueous vapour in the drift gas reduce the Lorentz angle.

Gas	range of drop	relative B-field dependence drop	
		0.8 vs. 0.0 Tesla	0.6 vs. 0.0 Tesla
DATCHA gas	0 to 4600 ppm	$\approx 24\,\%$	$\approx 18\,\%$
DATCHA gas	0 to 2000 ppm	$\approx 18\,\%$	$\approx 16\,\%$
four component gas	0 to 2600 ppm	$\approx 20\,\%$	$\approx 14\,\%$
four component gas	0 to 1500 ppm	$\approx 15\,\%$	$\approx 11\,\%$

Table 3: Relative drop of the B-field dependence

4.4 Resolution drop due to water content instabilities

We performed a calculation of the resolution drop due to an absolute and relative water content instability. In the first case Δw in equation 4 was a constant, while in the second Δw was a function of w: $\Delta w = c \cdot w$, where c is a constant. The results for both gases are shown in figures 18 to 21. The DATCHA gas has a minimum in the resolution contribution at the same water content as that at which the maximum drift time has a minimum. In this minimum the dependence of the rt-relation on the water content is so weak, that the RMS difference would stay below 10 μm even for a water content variation of 120 ppm or a relative stability of 7 %. For the four component gas no clear minimum was found, but a relative stability of 3% over a wide range of water contents would keep the RMS difference below 10 μm. Similar results have been obtained for the same calculation with a magnetic field of up to 0.8 Tesla.

5 Conclusion

The experiment confirms the assumptions about the drift properties of MDT gases at small water contents as well as the disagreement with the simulation. In particular a significant

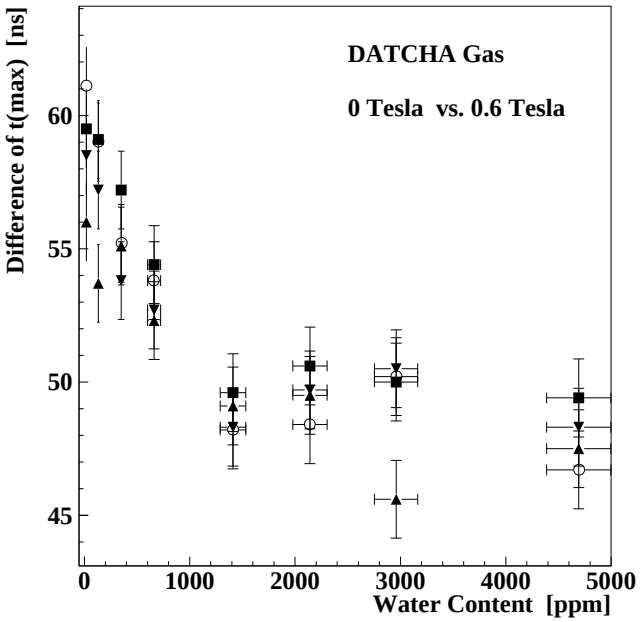

Figure 14: Reduction of magnetic field dependence at 0.6 Tesla through water for the DATCHA gas. The various symbols represent measurements from different tubes.

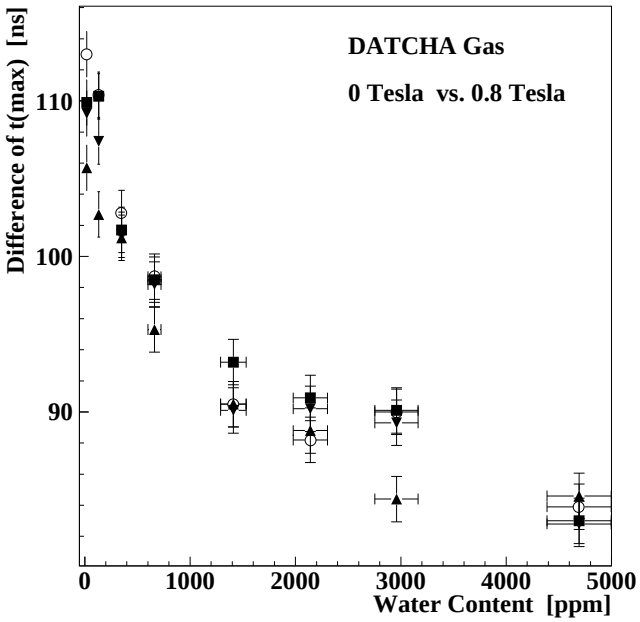

Figure 15: Reduction of magnetic field dependence at 0.8 Tesla through water for the DATCHA gas. The various symbols represent measurements from different tubes.

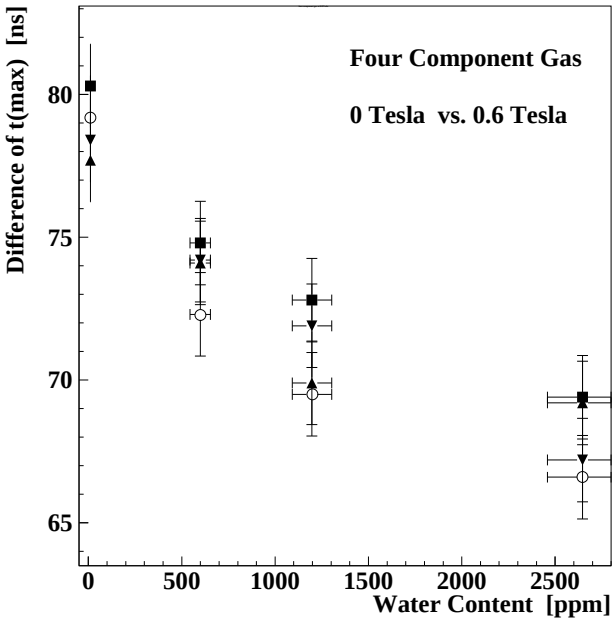

Figure 16: Reduction of magnetic field dependence at 0.6 Tesla through water for the four component gas. The various symbols represent measurements from different tubes.

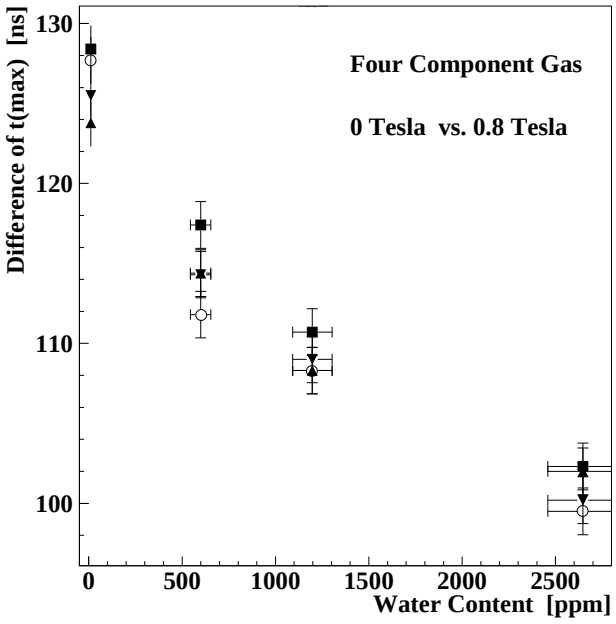

Figure 17: Reduction of magnetic field dependence at 0.8 Tesla through water for the four component gas. The various symbols represent measurements from different tubes.

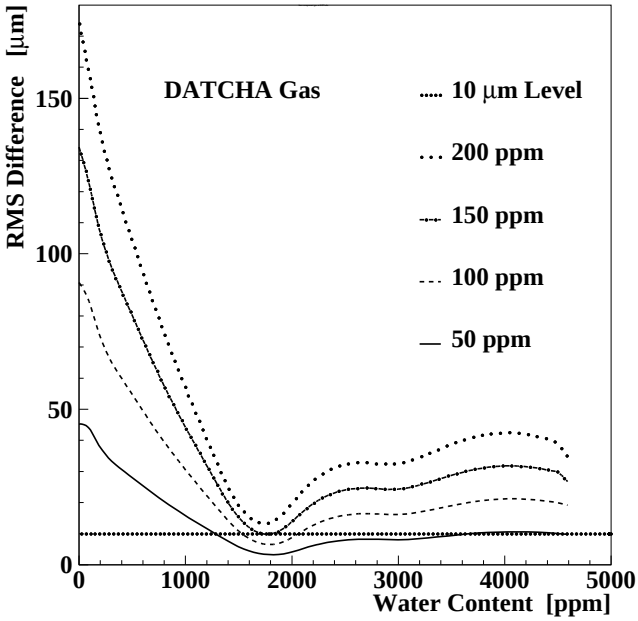

Figure 18: Resolution drop due to an absolute water content instability of 50 to 200 ppm for the DATCHA gas at 0.0 Tesla.

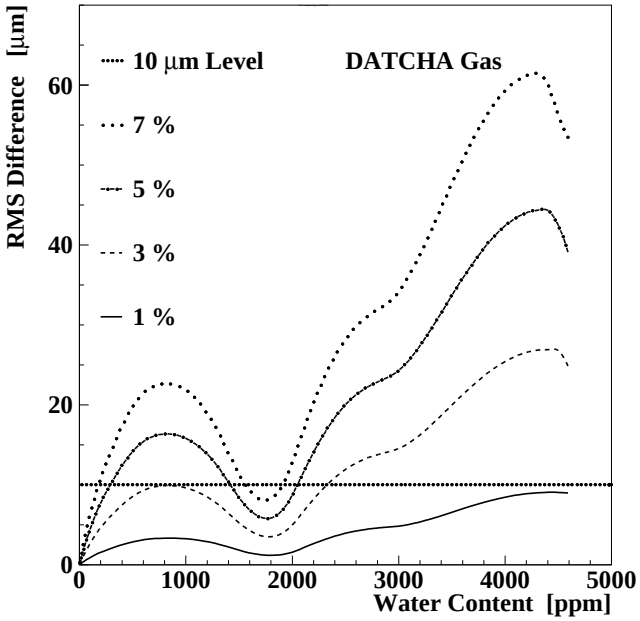

Figure 19: Resolution drop due to a relative water content instability of 1 % to 7 % for the DATCHA gas at 0.0 Tesla.

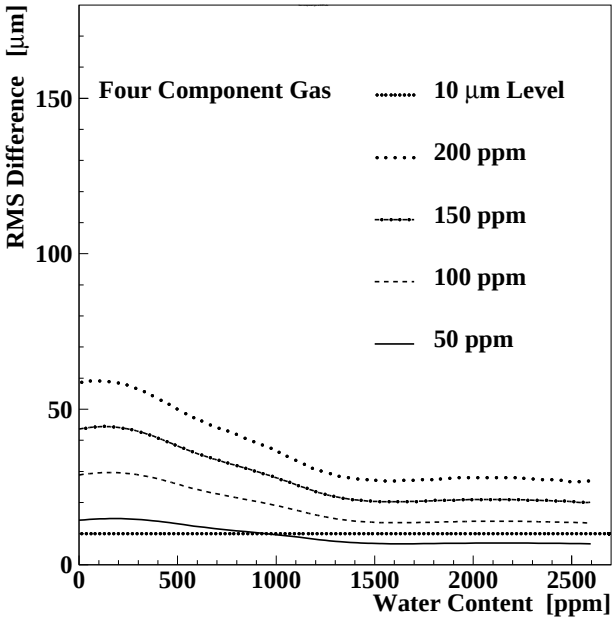

Figure 20: Resolution drop due to an absolute water content instability of 50 to 200 ppm for the four component gas at 0.0 Tesla.

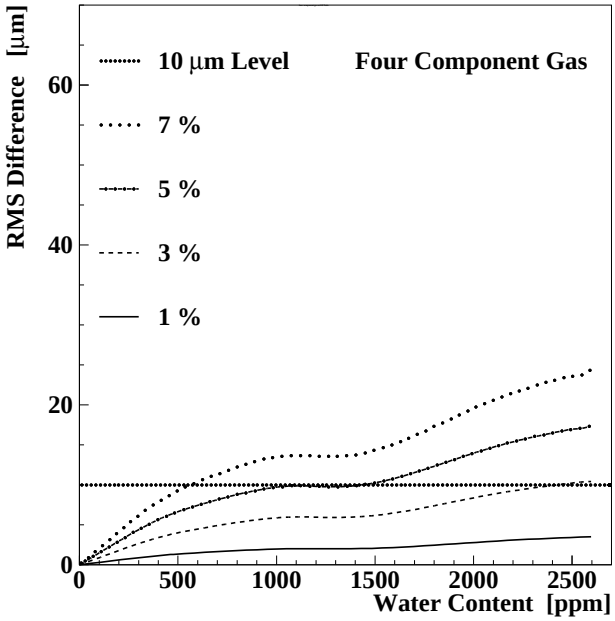

Figure 21: Resolution drop due to a relative water content instability of 1 % to 7 % for the four component gas at 0.0 Tesla.

reduction of the Lorentz angle through water could be demonstrated. The DATCHA gas is different from the four component gas in the sense that all drift property minima (maximum drift time at different B-fields, contribution to the resolution drop) show up at ≈ 1800 ppm. For the four component gas the minima of the maximum drift time at different magnetic fields are distributed over ≈ 600 ppm and the contribution to the resolution drop due to instabilities of the water content is, in the range that we investigated, a broad plateau, which does not lie in the range of the minima of the maximum drift time.
If one adds water vapour to the gases mentioned above the Lorentz angle and the maximum drift time decrease and the linearity of the rt-relation improves (up to a certain degree). The inevitable instability of the water content and hence the contribution to the resolution drop can be kept below 10 μm, if the stability is better than 3 %.
Based on these results the water content of the four component gas in the Freiburg ageing setup was set to 1500 ppm.

Acknowledgements

We would like to thank S. Veneziano and G. Polesello for the setup and the maintenance of the H8 DAQ system and R. Veenhof for his instructive comments. We highly appreciated the technical help by Charles Gruhn and Jean-Marc Demolis.

References

[DUBB96] Jörg Dubbert, *Bestimmung der Ortsauflösung von Hochdruckriftrohren für das Myon-Spektrometer des* ATLAS-*Experimentes*, Diplom Thesis, University of Munich, 1996.

[HILD95] M. Hildebrand, Universität Heidelberg, private communication, 1995.

[KADY90] J. A. Kadyk, *Wire chamber aging*, Nucl. Instr. and Meth. A300 (1991) 436-479.

[KEME95] P. I. Kemenes, Universität Heidelberg, private communication, 1995.

[KOLL96] M. Kollefrath & V. Paschhoff, *Influence of Rilsan hoses to the contents of H_2O (and O_2) in gas*, Talk given in the Detector physics meeting at CERN (1996)*.

[MN122] Mario Deile et al., *Test Beam Studies of the Gas Mixtures (...) for Drift Tubes*, ATLAS Internal Note Muon Note 122 (1996).

[MN137] Werner Riegler, *MDT MDT Resolution Simulation Frontend Electronics Requirements*, ATLAS Internal Note Muon Note 137 (1997).

[MN158] A. Negri et al., *Measurement of the maximum drift time in the Calypso MDT chamber*, ATLAS Internal Note Muon Note 158 (1997).

[MTDR97] ATLAS-Muon Collaboration, ATLAS-*Muon Spectrometer Technical Design Report*, 1997.

[SAMM97] Thomas Sammer, *Autokalibration von Driftrohrkammern für das* ATLAS-*Myonspektrometer*, Diplom Thesis, University of Munich, 1997.

[VEEN97a] R. Veenhof, GARFIELD, CERN Program Library (V6.14) (1997).

[VEEN97b] R. Veenhof, private communication 1997.

*Currently available under: ftp://hpfrs6.physik.uni-freiburg.de/atlas/dist/ba02_gas_water_paschhoff_jan96.eps.gz